Chemistry of new particle formation and growth events during wintertime in suburban area of Beijing : Insights from highly polluted atmosphere

Yang, Shuanghong

2021-06-15

1 **Chemistry of new particle formation and growth events during wintertime in suburban area of Beijing: insights from highly**

2 **polluted atmosphere**

3 Shuanghong Yang [a,b], Zirui Liu [b, f, g*], Petri S Clusius [c], Yongchun Liu [a], Jianan Zou [b], Yuan Yang [b], Shuman Zhao [b], Guozhong Zhang [b], Zhongjun Xu [a*],

4 Zhiqiang Ma [d], Yang Yang [e], Jie Sun [b], Yuepeng Pan [b], Dongsheng Ji [b], Bo Hu [b], Chao Yan [c], Michael Boy [c], Markku Kulmala [c], Yuesi Wang [b, f, g]

5 [a] *Department of Environmental Science and Engineering, Beijing University of Chemical Technology, Beijing 10029, China*

6 [b] *State key laboratory of Atmospheric Boundary Layer Physics and Atmospheric Chemistry (LAPC), Institute of Atmospheric Physics, Chinese Academy of*

7 *Sciences, Beijing 100029, China*

8 [c] *Institute for Atmospheric and Earth System Research/Physics, Faculty of Science, University of Helsinki, P.O. Box 64, 00014 University of Helsinki, Helsinki,*

9 *Finland*

10 [d] *Institute of Urban Meteorology, China Meteorological Administration, Beijing, China*

11 [e] *Weather Modification Office of Hebei Province, Shijiazhuang, China*

12 [f] *Center for Excellence in Regional Atmospheric Environment, Institute of Urban Environment, Chinese Academy of Science, Xiamen 361021, China*

13 [g] *University of Chinese Academy of Science, Beijing 100049, China*

14 [*]Correspondence liuzirui@mail.iap.ac.cn; xuzj@mail.buct.edu.cn

15

16 **Abstract:** The high frequency of new particle formation (NPF) events observed under polluted atmospheric conditions is still poorly

17 understood. To improve our understanding of NPF and its effects, the particle number size distribution (3-1000 nm) and submicron particle

18 chemical composition were measured from 4 November 2017 to 17 January 2018 in suburban Beijing. During this intense campaign, 22

19 NPF events were identified with a frequency of 29%, including 11 cases that occurred under "clean" conditions (C-NPF) and 11 cases that

20 occurred under "polluted" conditions (P-NPF). The observed formation rate (J_3) and condensation sink were 4.6-148.9 $cm^{-3} \cdot s^{-1}$ and 0.01-

21 0.07 s^{-1}, and the majority of NPF events occurred when the condensation sink (CS) values below 0.03 s^{-1}, indicating that condensation

22 vapor likely constitutes the critical limiting factor for NPF events. The correlations between log J_3 and [H_2SO_4] that close to previous

23 CLOUD experimental results in the majority of NPF events (68%) suggest the high nucleation rates (up to 100 $cm^{-3} \cdot s^{-1}$) would be attributed

24 by the amines that enhancing sulfuric acid nucleation, while the reminding cases (32%) possibly attributed to the H_2SO_4-NH_3 clustering

25 mechanism, which is supported by the theoretical expectations for H_2SO_4 nucleation with NH_3 simulated by the MALTE_BOX model. The

26 observed growth rate varied from 4.9 to 37.0 $nm \cdot h^{-1}$, with the dominant contribution (>60%) from sulfuric acid during the early phases of

27 growth (~4 nm), which was also sufficient to explain the observed Q_{GR} for <10 nm particles in high Q_{SO4} cases. While for the low sulfate

28 production (Q_{SO4}<0.1 $\mu g \cdot m^{-3} \cdot h^{-1}$) cases, Q_{SO4} systematically underestimated Q_{GR}, and the Q_{SO4}/Q_{GR} ratio drops from 0.5 to 0.3 as particles

29 grow from a 5-10 nm size range to a 15-20 nm size range, suggesting the condensation of organic compounds strengthened as the particles

30 grew larger and dominated the growth from 4 nm up to climatically relevant sizes (>50 nm).

31 **Keywords**: new particle events; formation mechanism; growth chemistry; polluted atmosphere

32

1. Introduction

34   Aerosol particles absorb solar radiation, scatter light, participate in cloud droplets formation by condensation, and change the

35 atmospheric trace gas levels via the processes of heterogeneous and multiphase reactions (Pöschl, 2005). A central phenomenon associated

36 with atmospheric aerosols is the newly formed particles and subsequently growth to ambient particle sizes. These processes are related to

37 a wide variety of events and have been observed nearly worldwide (Yu et al., 2016; Kerminen et al., 2018). In particular, new particle

38 formation (NPF) events are continually being reported in severely polluted backgrounds throughout China, and the intensity and frequency

39 of NPF events therein are reported to ranging between 10% to 50% (Chu et al., 2019), which was even higher than those in clean or

40 moderately polluted environments (Herrmann et al., 2014; Z. B. Wang et al., 2015; M. Hu et al., 2016; Lyu et al., 2018; Yao et al., 2018).

41 Additionally, the high nucleation rate (~80 $cm^{-3} \cdot s^{-1}$) reported in the polluted atmosphere can hardly be explained by classical homogenous

42 nucleation theory and the nucleation of sulfuric acid (H_2SO_4) particles suggested to be limited by the other alkaline gaseous species, for

43 instance, NH$_3$ (ammonia, Ball et al., 1999), DMA (amines) and oxidized organic compounds (R. Zhang et al., 2009; Metzger et al., 2010).

44 However, this kind of H$_2$SO$_4$-base mechanism is still barely reported in the field observation, especially for the polluted atmosphere cases.

45   The North China Plain (NCP), as one of the highest anthropogenically polluted areas in the world, is characterized by abundant gas-

46 phase pollutants (e.g., NH$_3$, VOCs, and SO$_2$) (Gu et al., 2014; Wu et al., 2017). To prevent further deterioration of air quality since 2013;

47 the toughest-ever "Air Pollution Prevention and Control Action Plan" has been implemented by the State Council of China to improve the

48 air quality nationwide. Subsequently, in the following five years (2013–2017), a reduction of 25% for PM$_{2.5}$ was found in the NCP region

49 (Zhang et al., 2019). NPF has been regarded as an important source of PM$_{2.5}$, and the newly formed particles and subsequent growth were

50 suggested to be the key contributor to fine particle pollution episodes in urban areas of North China (Guo et al., 2014). The significance of

51 ammonia in nucleation has been verified by previous chamber studies and theoretical works (Napari et al., 2002; Chon et al., 2014; Ortega

52 et al., 2008; Yu et al., 2017). Recently, the Cosmics Leaving Outdoor Droplets (CLOUD) chamber study using atmospheric levels of H$_2$SO$_4$

53 (10^5-10^8 molecules·cm^{-3}) and ammonia (~1 ppbv) successfully reproduced high NPF formation rates that comparable to the field

54 observations (Kürten et al., 2019), again supported the unique role of ammonia in enhancing sulfuric acid (SA) cluster formation. In

55 opposite, recent field studies indicate that the high nucleation rate observed in winter Shanghai were mainly attributed by the dimethylamine

56 (DMA) that enhancing sulfuric acid nucleation (Yao et al., 2018), while another NPF study showed the important role of dicarboxylic acids

57 participated in aerosol nucleation process in rural NCP (Fang et al., 2020). These results indicated the mechanism of NPF varied in different

58 field observations and chamber studies and still be poorly understood for the polluted atmosphere.

59   In addition, current understanding on the subsequent continuous aerosol particle growth during pollution episodes remains highly

60 uncertain. High concentrations of atmospheric trace gases (e.g. SO$_2$, NOx, NH$_3$) and VOCs were reported in pollution episodes in China

61 (L. Wang et al., 2011) and other highly polluted environment in Asia (Bighnaraj et al., 2018). These compounds like sulfuric acid and

62 HOMs are regarded as the main contributor to the secondary aerosol formation, which may have a similar contribution to aerosol growth

63 during pollution episodes (R. Zhang et al., 2015). Previous studies showed that the low-volatility organic vapors could be a major

64 contributor to the initial growth of nanoparticles during the midday and afternoon periods characterized by relatively intense

65 photochemistry (Paasonen et al., 2010; Liu et al., 2013). These low-volatility organic vapors can be produced from biogenic or

66 anthropogenic VOCs (Shilling et al., 2013; Setyan et al., 2014), and further oxidized to secondary organic aerosol (SOA) as reported in the

67 NCP region (Li et al., 2016). The emissions of VOCs were predicted to be still rising in recent years in China, which is much higher than

68 that in developed countries (H. Zhang et al., 2017; Sun et al., 2018). In addition, the composition of VOCs in Chinese cities is also largely

69 different from that in urban atmosphere of developed countries, which would result in the distinct role of HOMs in the particle growth (Qi

70 et al., 2018). However, such observations are still limited in the polluted regions of China. Therefore, sufficient field observation on NPF

71 is needed to better understand the potential nucleation mechanism that contributed to the high frequency of NPF events observed under

72 polluted atmospheric conditions.

73   In this study, an intensive field campaign focus on the atmospheric nucleation and growth processes were conducted at a highly

74 polluted suburban area of the NCP. The occurrence of NPF events and the formation rate of new particles, CS, and the growth rates (GR)

75 were reported and compared with previous findings performed in clean and polluted atmospheric environments. Additionally, the potential

76 nucleation mechanisms and the chemical species during the growth processes of nanoparticles were investigated in the polluted atmospheric

77 environment.

78 **2. Materials and methods**

79 **2.1. Observational station**

80   The intensive field observation campaign was actively carried out from Nov. 4th, 2017, to Jan. 17th, 2018 at the Xianghe suburban site

81 (39°47'5" N, 116°57'28" E), which located between the megacities of Beijing and Tianjin, and represent a typical suburban site in NCP.

82 The sampling station is about 4 km west of the downtown center and is surrounded by residential areas and agricultural land (see Fig. 1),

83 which experiences frequent the local primary emissions from biomass burning and coal combustion for domestic heating during wintertime

84 (Ran et al., 2016; Liu et al., 2018). The measurements were performed at the rooftop of an observation platform (roughly 10 m above

85 ground level).

86 **2.2. Measurement and instrumentation**

87 Size distributions of aerosol particle number (from 3 to 1000 nm in mobility diameter, dm) were gained by the combination of scanning

88 mobility particle spectrometers (SMPS, TSI Inc., USA) and a TSI aerosol particle sizer (APS3321), and submicron aerosols chemical

89 compositions (from 30 to 1500 nm in vacuum dynamic diameter) were obtained by an Aerodyne high-resolution time-of-flight aerosol

90 mass spectrometer (HR-ToF-AMS) (Liu et al., 2014). Ambient NH_3 was measured with a Picarro G1103 Analyzer at a high temporal

91 resolution (~5 s) (Benedict et al., 2018). The NH_3 detection limit (DL) was approximately 1 ppbv with a 3 min integration time. In addition,

92 the gaseous species and particulate matter (O_3, $NO/NO_2/NOx$, CO, SO_2, $PM_{2.5}$), and meteorological parameters (temperature, relative

93 humidity, wind speed/direction, solar radiation, etc.) were measured using the commercial instruments. More detailed descriptions about

94 these instruments and their calibration procedures were provided in the supporting information and were also presented in our previous

95 studies (Liu et al., 2016; Yang et al., 2019).

96 **2.3 Data processing**

97 **2.3.1 Aerosol dynamic modeling**

98 For the nucleation mode, the measured particle size limits of the SMPSs were extended down to 3 nm in our study. Due to low tubing

99 penetration efficiencies, the calculated atmospheric particle formation rate (J_3), defined as the flux of particles growing to over 3 nm in

100 size, can be calculated by considering the coagulation losses (CoagS) and growth losses (Sihto et al., 2006; Nieminen et al., 2011; Kulmala

101 et al., 2012):

102 $$J_3 = \frac{dN_{3\sim6}}{dt} + CoagS \cdot N_{3\sim6} + GR_{3\sim6} \cdot n_{3\sim6}$$

103 where $CoagS \cdot N_{3\sim6}$ represents the particle coagulation losses in the range of 3 to 6 nm during NPF; and $GR_{3\sim6} \cdot n_{3\sim6}$ represents the upper flux

104 limit of particulate growth greater than 6 nm.

105 Observed particle GR can be expressed as:

106 $$GR = \frac{\Delta D_m}{\Delta t}$$

107 where D_m is a mean geometric diameter of log-normal ultrafine particle mode, which has been fitted to the number size distribution.

108 CS can be described as (Kerminen et al., 2001):

109 $$CS = 2\pi D \int_0^\infty D_p \beta_M (D_p) n(D_P) dD_p = 2\pi D \Sigma_i \beta_M D_{p,i} N_i$$

110 where D is the diffusion coefficient; β_M is the correction factor of the transitional regime; N_i is the aerosol particle number concentration

111 in the size bin i; and $D_{p,i}$ is the particle diameter.

112 **2.3.2 Sulfuric acid proxy**

113 H_2SO_4 has been recognized as an essential gas-phase precursor in the nucleation process and subsequent growth of nano-sized particles

114 in the ambient atmosphere (Sipilä et al., 2010). In this study, the ambient H_2SO_4 concentration was estimated by a new proxy method

recently proposed by Dada et al. (2020), which takes into account the formation of sulfuric acid from SO_2 via OH oxidation and the oxidation of SO_2 via stabilized Criegee Intermediates:

$$\frac{d[H_2SO_4]}{dt} = k_1 GlobRad[SO_2] + k_2[O_3][Alkene][SO_2] - CS[H_2SO_4] - k_3[H_2SO_4]^2$$

Here, k_1 represents the coefficient of H_2SO_4 production term due to the SO_2 and OH reaction and k_2 is the coefficient of H_2SO_4 production via stabilized Criegree Intermediates (sCI) which are the alkenes ozonolysis productions. $CS[H_2SO_4]$ represents the loss of H_2SO_4 to pre-existing aerosol particles and $k_3[H_2SO_4]^2$ represents the loss of H_2SO_4 cluster formation. The coefficient values (k_1, k_2, k_3) used in this study were adopted from Dada et al. (2020) for the average values of the Beijing case (Table 2 therein). Note that the other three proxy methods had been previously reported and the more detailed description of three proxies was summarized in the supporting information (Petäjä et al., 2009; Mikkonen et al., 2011 and Lu et al., 2019; Fig. S1). To check if this new proxy could provide more accuracy of the H_2SO_4 concentration compared with the previous proxy methods, direct H_2SO_4 measurement data was used, which was obtained from a one-month winter campaign (January 2019) in Beijing detected by a Chemical Ionization atmospheric pressure interface time of flight spectrometer (CI-APi-ToF). As shown in Fig.S1, the new proxy proposed by Dada et al. (2020) predicts best the measured H_2SO_4 concentration and the other three proxy methods were largely overestimated or underestimated H_2SO_4 compared with the observation values.

2.3.3 Identify the chemical species contributed to the new particle growth

In order to explore the potential chemistry of nanoparticle growth, we applied a balance equation that established by Vakkari et al. (2015) to investigate the connections between secondary aerosol formation and new particle growth. During a new particle formation event, the change in submicron particle mass (Q_{AMS}) could be represented by different aerosol dynamical and atmospheric processes as follow:

$$Q_{AMS} = Q_{cond,kin} + Q_{cond,sv} + Q_{het} + Q_{trans}$$

Here, Q is regarded as the source rate of the atmospheric condensation vapor concentration (Kulmala et al., 2001a); $Q_{cond,kin} + Q_{cond,sv}$ accounted for the condensable vapors that contributed to the increase of submicron particle mass, Q_{het} represents the mass increase through heterogeneous formation pathways (Pöschl, 2011), and Q_{trans} represents changes in the submicron aerosol mass caused by air mass transport effects. The AMS measurements were used to calculate the sum of submicron aerosol mass increase rate (i.e., OA, SO_4^{2-}, NH_4^+, and NO_3^-) during the NPF event (Setyan et al., 2014; Vakkari et al., 2015), while the source rate of condensable vapors that needed to maintain the observed GR (Q_{GR}) and the observed J_3 (Q_{J3}) were calculated from the SMPS measurements (Kulmala et al., 2012). An example of a NPF event with simultaneous SMPS and AMS measurements is displayed in Figure S2. More details about this method were provided in our recent work (Yang et al., 2021) and also could be found in Vakkari et al. (2015).

3. Results and Discussion

3.1. Overview of the campaign

During the three-month winter field observation, the average values of temperature and RH were 1.0 ± 4.0 °C and 38 ± 18%, respectively. Stagnant conditions were frequently observed, with low wind speed days (< 2 m·s^{-1}) contributed roughly 75% of the entire observations, which constantly associated with weak wind from the south and southeast directions. Average concentrations of PM$_{2.5}$, NOx, and SO_2 were 71.0± 62.0 μg·m^{-3}, 70± 65 ppbv, and 6±5 ppbv, respectively, comparable to previous measurements in the suburban areas of the NCP (Kong et al., 2016) but much higher than those observed in urban Beijing (IAP site, approximately 50 μg·m^{-3}), which was consistent with our previous study that fine particle pollution in the suburban site (Xianghe) is more serious than that in urban Beijing due to the intense local primary emissions and pollutants transported from nearby megacities (Liu et al., 2018).

151   Variations of Aerosol particle number size distributions of 3-1000 nm during the campaign were presented in Fig. 2. Much higher

152   number concentrations were mainly present in the size range of 20-300nm. To better characterize the different sources of these submicron

153   aerosols, the measured particles are further divided into three modes: Nucleation mode (Nuc. 3-20nm), Aitken mode (Ait. 20-100nm), and

154   Accumulation mode (Acc. 100-1000nm). As showed in Fig. S3, similar diurnal variations of the Aitken mode and accumulation mode

155   particles were observed; both of which displayed the morning peak and evening peak during the rush hours, and suggesting the important

156   contribution from the traffic emissions (Wu et al., 2008; Liu et al., 2014). Notably, the morning peak of the Aitken mode particles was

157   weaker than that of the evening peak, suggesting other primary sources except the traffic emissions could also contribute to the increase of

158   Aitken mode particles during the evening rush hours, which would be relevant to the increase of biomass burning activity as showed in

159   Fig. S4. In fact, a large proportion of Aitken mode particles had been found to be originated from the primary combustion sources such as

160   biomass burning (Liu et al., 2014; Liu et al., 2017). Additionally, a unimodal distribution that peaked at midday (approximately 13:00 h,

161   local time) was observed for the nucleation mode particles. This phenomenon would be attributed to the nucleation mode formation and

162   subsequent growth under the strong solar radiation around noontime that favors the formation of gaseous precursors (Gao et al., 2012; Liu

163   et al., 2017; Ma et al., 2016).

3.2 General characteristics of NPF events

165   In this study, NPF events were identified by a burst particle number concentrations in the nucleation mode; an NPF event was

166   recognized if the duration time of the surge in the concentration of nucleation mode particles lasted for more than 2.5 h and if the maximum

167   of nucleation mode number concentrations exceeded 10^4 cm^{-3} (Wu et al., 2008). Twenty-two NPF events were detected, which contributed

168   to approximately 29% of the total observation period (Fig. 2). Generally, relatively lower concentrations of primary gaseous pollutants and

169   fine particles, lower RH but the higher wind speed was found in NPF days, compared with the non-NPF days (Table 1). These NPF events

170   usually appeared in the morning, and then formed nanoparticles continued to grow in the afternoon, and some NPF cases even continued

171   to grow in the evening (Fig. 3). Note that only the same period (09:00-16:00 h) for all the NPF cases instead of the whole day was considered

172   in Table 1, to make the comparison to be consistent as some NPF cases showed clearly nucleation mode particles around 09:00 and

173   continually growth only due to around 16:00. To explore the conditions that favored the occurrence of NPF, two types of these NPF events

174   were divided according to initial ambient PM$_{2.5}$ concentrations. As shown in Fig. 2b, eleven NPF events occurred at a relatively polluted

175   atmospheric environment with the high hourly PM$_{2.5}$ (> 75 μg·m^{-3}), which suggested polluted atmospheric conditions (P-NPF). In

176   comparison, the remaining eleven NPF events occurred at a relatively clean atmospheric environment with the hourly PM$_{2.5}$ concentrations

177   were below 35 μg·m^{-3} (C-NPF).

178   The formation rate values of 3 nm particles (J_3) were from 4.6 to 148.9 cm^{-3}·s^{-1} (09:00-12:00 h) in this study, which are largely higher

179   than those observed at a regional background station in NCP (4.9 cm^{-3}·s^{-1}, Z. Wang et al., 2013b) but comparable to those reported in the

180   urban sites (3.3-81.4 cm^{-3}·s^{-1}, Wu et al., 2008; 10-36 cm^{-3}·s^{-1}, Jayaratne et al., 2017), and those in the rural site (30.5-839.7 cm^{-3}·s^{-1}, Fang

181   et al., 2020) of North China Plain. Note that the J_3 values were only considered for the initial stage of the NPF events (09:00-12:00 h) as

182   the nucleation mode particles are formed clearly around 09:00, which was also consistent with the previous study wherein the J_3 values

183   only be considered for the initial stage of NPF (Wang et al., 2013). Interesting, the average J_3 (58.6 ±26.7 cm^{-3}·s^{-1}) during C-NPF events

184   was higher than that during P-NPF events (49.6 ±34.1 cm^{-3}·s^{-1}) under the similar sulfuric acid levels (Table 2), which probably due to the

185   lower CS values (0.01 ±0.003 s^{-1} vs. 0.03 ±0.02 s^{-1}) in C-NPF compared with P-NPF. Note that although the C-NPF days showed higher

186   average values of J_3 and GR and lower average values of H$_2$SO$_4$, NH$_3$ and CS than those observed in the P-NPF days, the difference was

187   not statistically significant for all the parameters present in Table 2. The observed CS values in this study were comparable to those of 0.01-

188   0.14 s^{-1} reported in urban Beijing (Gao et al., 2012; Wu et al., 2008; Jayaratne et al., 2017) and 0.03-0.10 s^{-1} observed in urban Shanghai

189   (Xiao et al., 2015). It is noted that the majority of NPF events occurred when the CS values below 0.03 s^{-1} (Fig. 4), while the CS values in

190   non-NPF days were generally larger than 0.03 s^{-1}, although the sulfuric acid levels were comparable between NPF and non-NPF days. In

191   addition, the higher formation rate (J_3) usually was associated with lower CS values. These results suggest that condensation vapor probably

192   constitutes the critical limiting factor for NPF events observed in suburban Beijing.

193   **3.3 Potential mechanisms for NPF events**

194   Reportedly, sulfuric acid is regarded as a critical participant among all the nucleation contributors in NPF events (Sipilä et al., 2010).

195   In these NPF events studies, the calculated H_2SO_4 concentration varied from 2.2×10^6 to 1.8×10^7 cm^{-3}, which was equivalent to those

196   reported in various urban sites of North China (Wu et al., 2008; Yue et al., 2010; Gao et al., 2012) and those reported in Shanghai (Yao et

197   al., 2018). However, the correlation coefficient between J_3 and [H_2SO_4] in this study (R=0.50 in C-NPF and R=0.46 in P-NPF) are lower

198   than those reported in urban stations, such as Beijing (R=0.92, Yue et al., 2010) and Shanghai (R=0.62, Xiao et al., 2015), which suggested

199   that the ambient sulfuric acid was insufficient accounting for the observed high nucleation rate in the present study. Nucleation of H_2SO_4

200   participation is acknowledged to be accelerated by the presence of other alkaline gaseous species, for instance, ammonia (Ball et al., 1999)

201   or organic compounds (i.e., amines or oxidized organic productions) (Metzger et al., 2010; R. Zhang et al., 2004, 2009).

202   To explore the potential mechanism of NPF in suburban Beijing, the relationship between J_3 and [H_2SO_4] in this study was compared

203   with two nucleation mechanisms (H_2SO_4-NH_3-H_2O and H_2SO_4-DMA-H_2O) obtained from the CERN-CLOUD experiments (Almeida et

204   al., 2013; Kürten, 2019). In these NPF events study, it is notable that the field observation conditions (274 ±3 K and 30 ±10% RH) are

205   extremely close to the CLOUD experimental conditions (278 K and 38% RH); hence, in this study, temperature and RH are not expected

206   to greatly strengthen the formation rates of nucleation mode particles during NPF events period at the suburban Beijing site (Paasonen et

207   al., 2012). As shown in Fig. 5a, the majority of our measured particle formation rates (68%, Group1) are close to those reported with

208   H_2SO_4-DMA-H_2O nucleation mechanisms under the ambient levels of sulfuric acid (10^6-10^7 cm^{-3}), consistent with the findings observed

209   at the megacity of Shanghai (Yao et al., 2018), indicating the high NPF formation rates (~100 cm^{-3}·s^{-1}) detected in the polluted suburban

210   site would be attributed by the DMA that enhancing sulfuric acid nucleation. Previous field studies conducted in clean regions (e.g. forested

211   areas) and polluted urban areas (e.g. urban Beijing) suggested the organic compounds (Yue et al., 2010), or highly oxygenated organic

212   molecules (HOMs) would enhance the nucleation (Ehn et al., 2014; Roldin et al., 2019). However, HOMs would not be the main contributor

213   in this study, as the formation of HOMs at our observation site would be largely inhibited by the reaction between RO_2 radicals and NO

214   due to the presence of high levels of NO*x* (~23 ppb) (Wildt et al., 2014). In addition, a recent field study conducted in the rural area of

215   North China Plain also suggested the involvement of dicarboxylic acids in particle nucleation via bonding with H_2SO_4, NH_3, amines, and

216   other molecules (Fang et al., 2020). However, whether the concentration of dicarboxylic acids is sufficient enough to participate in the

217   nucleation in our suburban site needed to be further confirmed from future field measurements that were unavailable in this study.

218   Note that there was a substantial amount of measured particle formation rates (32%, Group 2) that are not within the orbit of the

219   H_2SO_4-DMA-H_2O mechanism (Fig. 5a), suggesting another acidic or alkaline species may contribute to the enhanced sulfuric acid

220   nucleation. As showed in Fig.5a, this group showed approximately 10-fold lower [H_2SO_4] and 10-fold higher [NH_3] compared with the

221   H_2SO_4-NH_3-H_2O experiments (Kürten, 2019), although they share the comparable nucleation rate (10-100 cm^{-3}·s^{-1}). According to the

222   CLOUD experimental results in Fig. 5a, the formation rate of H_2SO_4 particles could be enhanced more than 100-fold when the ammonia

223   mixing ratio increased from sub-ppt conditions to up-ppb conditions. Furthermore, as reported by Kürten (2019), the enhancement of

224   ammonia would not reach a plateau toward a high ammonia concentration (approximately 4 ppbv) under atmospheric conditions (278 K

225   and 292 K), although a saturation threshold of ammonia to the increasing nucleation rate of sulfuric acid particles was observed under cold

226   conditions (<248 K). Thus, the much higher concentration of ammonia (approximately 14 ppbv) in the present study would be expected to

227   gain a similar nucleation rate even under lower sulfur acid conditions. As the CLOUD experiments have not yet performed under similar

atmospheric conditions as our field observation, MALTE-BOX modeling was performed using input parameters of fixed ammonia concentration (10 ppbv) and fixed parameters of CS (0.03 s^{-1}), temperature (275 K), RH (38%) and pressure (1011.66 hPa) that were close to the average conditions of NPF events. Through the simulations obtained by the Atmospheric Cluster Dynamics Code model (ACDC) coupled with MALTE-BOX (McGrath et al., 2012; Boy et al., 2006), the dependency of the NPF rates for varying sulfuric acid concentrations at fixed ammonia concentrations can be yielded. In Group 2, the measured particle formation rates are located within the band of the theoretical expectations for H_2SO_4-NH_3 clustering (Fig. 5a), although the nucleation rates values predicted by the MALTE-BOX model are higher than the experiment measured. This discrepancy might be caused by the smaller-sized clusters used in the model (the initial cluster contains five acid and five base molecules, corresponding to mobility diameters of 1.07 nm) (Huang et al., 2016), resulting in a higher formation rate. Furthermore, an apparent linear correlation between J_3 and [H_2SO_4] and [NH_3] concentration was shown in Group 2 (Fig. 5c). Pearson's correlation coefficient (R) was largely increased from 0.46-0.50 between J_3 and [H_2SO_4] to 0.84-0.91 between J_3 and [H_2SO_4] × [NH_3] (p<0.01). A similar close relationship between J_3 and [NH_3] was also observed in a previous study conducted in winter Shanghai (Xiao et al., 2015), where stronger linear correlations between $J_{1.34}$ and [NH_3] than between $J_{1.34}$ and [H_2SO_4] were observed (R^2: 0.62 vs. 0.38). Similarly, this kind of relationship was also reported in Atlanta with a sulfur-rich atmosphere (McMurry et al., 2005), while it was absent from atmospheric observations conducted in Kent, Ohio (Erupe et al., 2010). This difference possibly caused by the different concentrations of NH_3, which has been predicted to reach a discrimination threshold of saturation (Napari et al., 2002; Benson et al., 2009). In this study, the concentrations of NH_3 ranged from 5 to 32 ppbv during NPF events, which are comparable to those of 2-16 ppbv in winter Shanghai (Xiao et al., 2015) and those of 1-10 ppbv in Atlanta (McMurry et al., 2005) but largely higher than those in Kent, Ohio (Erupe et al., 2010), where the NH_3 concentration was reported to be at the sub-ppbv level. Although previous CLOUD experiments suggested that the ternary nucleation of NH_3-H_2SO_4-H_2O is unable to explain the observed atmospheric nucleation under the sub-ppbv level of ammonia (Kirkby et al., 2011), the recent CLOUD experiments successfully reproduced high NPF formation rates that comparable to the field observations under the up-ppb level of ammonia (Kürten, 2019). Thus, the abundance of ammonia observed in this study of more than 10-fold of the CLOUD experiments (up to 10 ppbv) would be sufficient to account for the atmospheric H_2SO_4-NH_3 cluster formation in the highly polluted suburban atmosphere. These field observation results, especially for theoretical expectations, show that ammonia could be enhanced H_2SO_4 clusters nucleation in Group 2 events, while for the Group 1 events, DMA would be played a dominant role in the enhanced sulfur acid nucleation. However, further evidence from direct measurements of atmospheric amines in suburban Beijing is needed to better understand the role of atmospheric amine in future NPF studies.

3.4 Influence of particle chemistry on new particle growth

In this study, the GR of nucleation particles ranged from 4.9 to 37.0 nm·h^{-1}, which is comparable to that of 1.7-21.1 nm·h^{-1} recorded in urban Shanghai (Xiao et al., 2015) and that of 3.2-13.5 nm·h^{-1} observed at rural sites in the NCP (Z. Wang et al., 2013b; Peng et al., 2014) but larger than that of 0.5-9.0 nm·h^{-1} observed in urban Beijing (Jayaratne et al., 2017). Moreover, the GR of nucleation particles (Table 2) was slightly higher during C-NPF events (15.1± 6.8 nm·h^{-1}) than during P-NPF events (14.6± 5.1 nm·h^{-1}) and was close to the upper limit of the GRs previously observed in urban areas (Peng et al., 2014), indicating the abundance of condensable vapors during the intensive field campaign. Interesting, the averaged GR was lower in the P-NPF events although the condensable vapors were expected to be higher than that in the C-NPF events. This phenomenon could be attributed to the competition of condensable vapours from the background aerosol as the particle concentrations were also much higher in the P-NPF events. The much higher CS values observed in the P-NPF events than in the C-NPF (0.03 s^{-1} vs 0.01 s^{-1}) also support the above hypothesis.

Nucleation mode particles must grow to the larger sized particle in short times to reduce the dynamic losses in minimum, which associated with coagulation scavenging between small particles and preexisting particles. H_2SO_4 and low volatility organic vapors were

266　believed to be the essential contributors to the particle continual growth originated from NPF events. In general, H_2SO_4 was identified as

267　a key contributor to nanoparticle growth but was implicit for subsequent growth to larger particles (Wang et al., 2015; Chu et al., 2019). In

268　this study, the relative contributions of H_2SO_4 were estimated to be 50%-70%, 20%-50%, and less than 20% for nanoparticles of 4-6 nm,

269　6-10 nm, and >10 nm, respectively (Fig. 6). Xiao et al. (2015) reported that the relative contributions of H_2SO_4 for nanoparticle growth in

270　urban Shanghai were 39% and 29% for nanoparticles of 2.4-7 nm and 7-20 nm, respectively, while a contribution of 3%-14% for the 7-30

271　nm particles was reported in an urban site of Beijing during an intense summer campaign (Wang et al., 2015). These results show the

272　significant role of H_2SO_4 in the growth of freshly nucleated particles (<10 nm); however, the observed growth rates of larger particles (>10

273　nm) were suggested as being dominated by species other than H_2SO_4 (Kuang et al., 2012; X. Liu et al., 2014; Meng et al., 2015).

274　　　To explore the particle chemistry on nucleated particle growth in more detail, the variations in submicron particle chemical components

275　measured by an HR-ToF-AMS during the NPF growth processes are analyzed. Notably, the submicron particle chemical components from

276　HR-ToF-AMS may not be directly relevant to the NPF particles. However, in the specific situations of NPF event when condensation of

277　gaseous vapor dominates the changes of submicron aerosol composition, the source rate for different chemical compounds that contributed

278　to new particle growth could be deduced from the time evolution of the chemical composition of the bulk submicron aerosol (Pierce et al.,

279　2011; Vakkari et al., 2015). Based on the Q_{GR}- Q_{AMS} theoretical frame that exploring the balance between the source rate of condensable

280　vapors and the observed growth rate of nanoparticles (Vakkari et al., 2015), the chemistry of particle growth during the special NPF case

281　were further investigated. Figure 7a-c shows a comparison between Q_{GR} and Q_{SO4} for three classified size ranges. The observed Q_{SO4} was

282　sufficient to explain the observed Q_{GR} for <10 nm particles in high Q_{SO4} cases, indicating that the growth of the smallest particles was

283　probably dominated by the atmospheric H_2SO_4 condensation reactions. Nevertheless, in cases with slow sulfate production (Q_{SO4}<0.1

284　$\mu g \cdot m^{-3} \cdot h^{-1}$), Q_{SO4} systematically underestimated Q_{GR}, suggesting that organic compounds were the primary contributor to nucleated

285　particles growth from the very beginning when Q_{OM} was dominant in these cases (hourly $PM_{2.5}$<35 $\mu g \cdot m^{-3}$, Fig. S5), the similar findings

286　have been reported in a boreal forest environment by Kulmala et al. (2012) and Ehn et al. (2014). Sulfuric acid was not enough to explain

287　the particle continual growth except in a few high Q_{SO4} cases (Q_{SO4}>1 $\mu g \cdot m^{-3} \cdot h^{-1}$, Figure 6b). On average, the Q_{SO4}/Q_{GR} ratio drops from

288　0.5 to 0.3 as particles grow from a 5-10 nm size range to a 15-20 nm size range (Fig. S6), suggesting that the condensation of organic

289　compounds strengthened as the particles grew larger. Actually, in most cases, the observed Q_{GR} for 10-20 nm particles could be explained

290　by the observed high values of Q_{OM} (Fig. 6e), especially in the cases of higher fractions of SOA. This phenomenon was different from

291　those observed in New Delhi, where the aerosol growth events was mainly contributed by the aqueous formation of sulfate during nighttime

292　(Bighnaraj et al., 2018). However, our results are consistent with previous studies that investigated the evolution of the size-resolved

293　chemical composition of new particles using AMS data, which showed the subsequent growth of nucleated particles was driven primarily

294　by the condensation of oxygenated organic species at the U.S. EPA Pittsburgh Supersite (Q. Zhang et al., 2004), a suburban area of

295　California (Setyan et al., 2014) and a rural site (Welgegund station) in South Africa (Vakkari et al., 2015). These results highlight the

296　important role of organic compounds that enhance nucleated particle growth to climatically relevant sizes (>50 nm) in both the clean

297　atmosphere and the polluted urban environment.

298　**4. Conclusion**

299　　　An intensive field campaign focus on the atmospheric nucleation and growth processes were conducted at a highly polluted suburban

300　area of the North China Plain (NCP). During the three-month winter campaign, twenty-two new particle formation (NPF) events were

301　detected with half of them occurred under "clean" conditions (C-NPF) and the rest occurred under "polluted" conditions (P-NPF). The

302　mean formation rate of 3 nm particles (J_3) ranged from 4.6 to 148.9 $cm^{-3} \cdot s^{-1}$, which are largely higher than those observed at regional

303　background sites but comparable to those reported in the urban and rural sites located in North China Plain. In addition, the observed CS

values in this study were comparable to those of previous studies, and the condensation vapor probably constitutes the critical limiting factor for NPF events observed in suburban Beijing. The correlations between log J_3 and [H_2SO_4] that close to previous CLOUD experimental results for H_2SO_4-DMA-H_2O ternary nucleation in the majority of NPF events (68%), suggest the high NPF rates (up to 100 $cm^{-3} \cdot s^{-1}$) would be attributed by the amines that enhancing sulfuric acid nucleation. Whereas, the reminding NPF cases (32%) was suggested to be attributed to the H_2SO_4-NH_3 clustering mechanism, which is supported by the theoretical expectations for H_2SO_4 nucleation with NH_3 simulated by the MALTE_BOX model under the similar conditions of the field observations. The observed growth rate was found to be mainly contributed by sulfuric acid (>60%) during the early phases of growth (~4 nm), which was also sufficient to explain the observed Q_{GR} for <10 nm particles in high Q_{SO4} cases. While for the low sulfate production (Q_{SO4}<0.1 $\mu g \cdot m^{-3} \cdot h^{-1}$) cases, Q_{SO4} systematically underestimated Q_{GR}, and the Q_{SO4}/Q_{GR} ratio drops from 0.5 to 0.3 as particles grow from a 5-10 nm size range to a 15-20 nm size range, suggesting the condensation of organic compounds strengthened as the particles grew larger and dominated the growth from 4 nm up to climatically relevant sizes (>50 nm). Future studies are needed for molecular-scale measurements of organic vapors and chemical property of nucleation mode particles, to fully understand the chemistry of new particle growth in the polluted North China Plain.

References

Almeida, J., Schobesberger, S., Kurten, A., Ortega, I. K., Kupiainenmaatta, O., Praplan, A. P., Adamov, A., Amorim, A., Bianchi, F., Breitenlechner, M., David, A., Dommen, J., Donahue, N. M., Downard, A. J., Dunne, E. M., Duplissy, J., Ehrhart, S., Flagan, R. C., Franchin, A., Guida, R., Hakala, J., Hansel, A., Heinritzi, M., Henschel, H., Jokinen, T., Junninen, H., Kajos, M. K., Kangasluoma, J., Keskinen, H., Kupc, A., Kurten, T., Kvashin, A. N., Laaksonen, A., Lehtipalo, K., Leiminger, M., Leppa, J., Loukonen, V., Makhmutov, V. S., Mathot, S., Mcgrath, M., Nieminen, T., Olenius, T., Onnela, A., Petaja, T., Riccobono, F., Riipinen, I., Rissanen, M. P., Rondo, L., Ruuskanen, T., Santos, F. D., Sarnela, N., Schallhart, S., Schnitzhofer, R., Seinfeld, J. H., Simon, M., Sipila, M., Stozhkov, Y. I., Stratmann, F., Tome, A., Trostl, J., Tsagkogeorgas, G., Vaattovaara, P., Viisanen, Y., Virtanen, A., Vrtala, A., Wagner, P., Weingartner, E., Wex, H., Williamson, C., Wimmer, D., Ye, P., Ylijuuti, T., Carslaw, K. S., Kulmala, M., Curtius, J., Baltensperger, U., Worsnop, D. R., Vehkamaki, H., and Kirkby, J., 2013. Molecular understanding of sulphuric acid-amine particle nucleation in the atmosphere. Nature. 502, 359-363.

Ball, S. M., Hanson, D. R., Eisele, F. L., and McMurry, P. H., 1999. Laboratory studies of particle nucleation: initial results for H_2SO_4, H_2O, and NH_3 vapors. J. Geophys. Res. 104, 23709-23718.

Benedict, K. B., Prenni, A. J., Sullivan, A. P., Evanoskicole, A. R., Fischer, E. V., Callahan, S., Sive, B. C., Zhou, Y., Schichtel, B. A., and Collett Jr. J. L., 2018. Impact of Front Range sources on reactive nitrogen concentrations and deposition in rocky mountain national park. PeerJ. 6(5), 1-26.

342 Benson, D. R., Erupe, M. E., and Lee, S. H., 2009. Laboratory-measured H_2SO_4-H_2O-NH_3 ternary homogeneous nucleation rates: Initial

343   observations. Geophys. Res. Lett. 36, L15818.

344 Bighnaraj, S., Shankar, G. A., Bhagawati, K., Sudhanshu, K., Ravleen, K., Deepak, S., Suresh, T., Kimitaka, K., 2018. Nighttime particle

345   growth observed during spring in New Delhi: Evidence for the aqueous phase oxidation of SO_2. Atmos. Environ., 188, 82-96.

346 Boy, M., Hellmuth, O., Korhonen, H., Nilsson, E. D., ReVelle, D., Turnipseed, A., Arnold, F., and Kulmala, M., 2006. MALTE-model to

347   predict new aerosol formation in the lower troposphere. Atmos. Chem. Phys. 6, 4499-4517.

348 Chon, N. L., Lee, S. H., Lin, H., 2014. A theoretical study of temperature dependence of cluster formation from sulfuric acid and ammonia.

349   Chem. Phys. 433, 60-66.

350 Chu, B. W., Kerminen, V. M., Bianchi, F., Yan, C., Petäjä, T., Kulmala, M., 2019. Atmospheric new particle formation in China. Atmos.

351   Chem. Phys. 19(1), 115-138.

352 Dada, L., Ylivinkka, I., Baalbaki, R., Li, C., Guo, Y., Yan, C., Yao, L., Sarnela, N., Jokinen, T., Daellenbach, K. R., Yin, R., Deng, C., Chu,

353   B., Nieminen, T., Kontkanen, J., Stolzenburg, D., Sipilä, M., Hussein, T., Paasonen, P., Bianchi, F., Salma, I., Weidinger, T., Pikridas,

354   M., Sciare, J., Jiang, J., Liu, Y., Petäjä, T., Kerminen, V.-M., Kulmala, M. 2020. Sources and sinks driving sulphuric acid

355   concentrations in contrasting environments: implications on proxy calculations, Atmos. Chem. Phys. 20, 11747–11766.

356 Ehn, M., Thornton J. A., Kleist E., Sipilä, M., Junninen, H.i., Pullinen, I., Springer, M., Rubach, F., Tillmann, R., Lee, B., Lopez-Hilfiker,

357   F., Andres, S., Acir, I.H., Rissanen, M., Jokinen, T., Schobesberger, S., Kangasluoma, J., Kontkanen, J., Nieminen, T., Kurtén, T.,

358   Nielsen, L.B., Jørgensen, S., Kjaergaard, H.G., Canagaratna, M., Maso, M.D., Berndt, T., Petäjä, T., Wahner,A., Kerminen, V.M.,

359   Worsnop, D. R., Wildt, J., Mentel, T.F., Kulmala M., 2014. A large source of low-volatility secondary organic aerosol. Nature.

360   506(7489), 476-479.

361 Erupe, M. E., Benson, D. R., Li, J., Young, L. H., Verheggen, B., Tahboub, O., Cunningham, V., Frimpong, F., Viggiano A.A., Lee, S.H.,

362   Al‑Refai, M., 2010. Correlation of aerosol nucleation rate with sulfuric acid and ammonia in Kent, Ohio: An atmospheric

363   observation. J. Geophys. Res.: Atmos. 115(D23216), 1-18.

364 Fang, X., Hu, M., Shang, D., Tang, R., Shi, L., Olenius, T., Wang, Y., Wang, H., Zhang, Z., Chen, S., Yu, X., Zhu, W., Lou, Sh., Ma, Y., Li,

365   X., Zeng, L., Wu, Z., Zheng, J., and Guo, S., 2020. Observational Evidence for the Involvement of Dicarboxylic Acids in Particle

366   Nucleation. Environ. Sci. Technology Lett. 7 (6), 388-394.

367 Gao, J., Chai, F., Wang, T., Wang, S., Wang, W., 2012. Particle number size distribution and new particle formation: New characteristics

368   during the special pollution control period in Beijing. J. Environ. Sci., 24(1), 14-21.

369 Gu, B., Sutton, M. A., Chang, S. X., Ge, Y., Chang, J., 2014. Agricultural ammonia emissions contribute to China's urban air pollution.

370   Frontiers in Ecology and the Environment. 12(5), 265-266.

371 Guo, S., Hu, M., Zamora, M. L., Peng, J., Zhang, R., 2014. Elucidating severe urban haze formation in China. Proc. Natl Acad. Sci., 111(49),

372   17373.

373 Herrmann, E., Ding, A. J., Kerminen, V. M., Petäjä, T., Yang, X.Q., Sun, J.N., Qi, X.M., Manninen, H., Hakala, J., Nieminen, T., Aalto,

374   P.P., Kulmala, M., Fu, C.B., 2014. Aerosols and nucleation in eastern China: first insights from the new SORPES-NJU station.

375   Atmos. Chem. Phys. 14(4), 2169-2183.

376 Hu, M., Shang, D., Guo, S., Wu, Z., 2016. Mechanism of New Particle Formation and Growth as well as Environmental Effects under

377   Complex Air Pollution in China. Acta Chim. Sin. 74, 385-39.

378   Huang, X., Zhou, L., Ding, A., Qi, X., Nie, W., Wang, Mi., Chi, X., Petaja, T., Kerminen, V., Roldin, P., Rusanen, A., Kulmala, M., and

379   Boy M., 2016. Comprehensive modelling study on observed new particle formation at the SORPES station in Nanjing, China.

380   Atmos. Chem. Phys. 16, 2477-2492.

381   Jayaratne, R., Pushpawela, B., He, C., Li, H., Gao, J., Chai, F., Morawska, L., 2017. Observations of particles at their formation sizes in

382   Beijing, China. Atmos. Chem. Phys. 17(14), 8825-8835.

383   Kerminen, V. M., Pirjola, L., Kulmala, M., 2001. How significantly does coagulational scavenging limit atmospheric particle production?

384   J. Geophys. Res.: Atmos. 106(D20), 24119-24125.

385   Kerminen, V. M., Chen, X., Vakkari, V., Petäjä, T., Kulmala, M., & Bianchi, F., 2018. Atmospheric new particle formation and growth:

386   review of field observations. Environ. Res. Lett. 13(10), 103003.

387   Kirkby, J. Curtius, J., Almeida, J., Dunne, E. M., Duplissy, J., Ehrhart, S., Franchin, A., Gagne, S., Ickes, L., Kurten, A., Kupc, A., Metzger,

388   A., Riccobono, F., Rondo, L., Schobesberger, S., Tsagkogeorgas, G., Wimmer, D., Amorim, A., Bianchi, F., Breitenlechner, M.,

389   David, A., Dommen, J., Downard, A. J., Ehn, M., Flagan, R. C., Haider, S., Hansel, A., Hauser, D., Jud, W., Junninen, H., Kreissl,

390   F., Kvashin, A. N., Laaksonen, A., Lehtipalo, K., Lima, J., Lovejoy, E. R., Makhmutov, V. S., Mathot, S., Mikkila, J., Minginette,

391   P., Mogo, S., Nieminen, T., Onnela, A., Pereira, P., Petaja, T., Schnitzhofer, R., Seinfeld, J. H., Sipila, M., Stozhkov, Y. I., Stratmann,

392   F., Tome, A., Vanhanen, J., Viisanen, Y., Vrtala, A., Wagner, P., Walther, H., Weingartner, E., Wex, H., Winkler, P. M., Carslaw, K.

393   S., Worsnop, D. R., Baltensperger, U., Kulmala M., 2011. Role of sulphuric acid, ammonia and galactic cosmic rays in atmospheric

394   aerosol nucleation. Nature. 476, 429-433.

395   Kong, L., Xin, J., Zhang, W., Wang, Y., 2016. The empirical correlations between $PM_{2.5}$, PM_{10} and AOD in the Beijing metropolitan region

396   and the PM2.5, PM10 distributions retrieved by MODIS. Environ. Pollut. 216, 350-360,.

397   Kuang, C., Chen, M., Zhao, J., Smith, J., McMurry, P. H., Wang, J., 2012. Size and time-resolved growth rate measurements of 1 to 5 nm

398   freshly formed atmospheric nuclei. Atmos. Chem. Phys. 12(7), 3573-3589.

399   Kulmala, M., M. Dal Maso, J. M. Mäkelä, L. Pirjola, M. Väkevä, P. Aalto, P. Miikkulainen, K. Hämeri, and C. D. O'Dowd., 2001a. On the

400   formation, growth and composition of nucleation mode particles, Tellus B. 53, 479–490.

401   Kulmala, M., Petäjä, T., Nieminen, T., Sipilä, M., Manninen, H. E., Lehtipalo, K., Maso, M.D., Aalto, P.P., Junninen, H., Paasonen, P.,

402   Riipinen, I., Lehtinen, K.E.J., Laaksonen, A., Kerminen, V.M., 2012. Measurement of the nucleation of atmospheric aerosol

403   particles. Nature Protoc. 7(9), 1651-1667.

404   Kürten, A., 2019. New particle formation from sulfuric acid and ammonia: nucleation and growth model based on thermodynamics derived

405   from CLOUD measurements for a wide range of conditions. Atmos. Chem. Phys. 19, 5033-5050.

406   Li, J. L., Zhang, M. G., Gao, Y., Chen, L., 2016. Model analysis of secondary organic aerosol over China with a regional air quality

407   modeling system (RAMS-CMAQ). Atmos. Ocean. Sci. Lett. 9(6), 443-450.

408   Liu, X. G., Li, J., Qu, Y., Han, T., Hou, L., Gu, J., Zhang, Y., 2013. Formation and evolution mechanism of regional haze: a case study in

409   the megacity Beijing, China. Atmos. Chem. Phys. 13(9), 4501-4514.

410   Liu, X. H., Zhu, Y. J., Zheng, M., Gao, H. W., Yao, X. H., 2014. Production and growth of new particles during two cruise campaigns in

411   the marginal seas of China. Atmos. Chem. Phys. 14(15), 7941-7951.

412   Liu, Z. R., Hu, B., Liu, Q., Sun, Y. and Wang, Y. S. 2014. Source apportionment of urban fine particle number concentration during

413   summertime in Beijing. Atmos. Environ. 96, 359-369.

414   Liu, Z., Hu, B., Zhang, J., Yu, Y., Wang, Y., 2016. Characteristics of aerosol size distributions and chemical compositions during wintertime

415   pollution episodes in Beijing. Atmos. Res., 168, 1-12.

416   Liu, Z. R., Hu, B., Zhang, J., Xin, J., Wu, F., Wang, Y., 2017. Characterization of fine particles during the 2014 Asia-Pacific economic

417   cooperation summit: Number concentration, size distribution and sources. Tellus B. 69(1), 1-19.

418   Liu, Z. R, Gao, W.K., Hu, B., Xin, J.Y., Sun, Y., Wang, L.L., Wang, G.H., Bi, X.H., Zhang, G.H., Xu, H, H., Cong, Z.Y., He, J., Xu, J.S.,

419   Wang, Y.S., 2018. Characteristics of $PM_{2.5}$ mass concentrations and chemical species in urban and background areas of China:

420   emerging results from the CARE-China network. Atmos. Chem. Phys. 18, 8849-8871.

421   Lu, Y., Yan, C., Fu, Y., Chen, Y., Liu, Y., Yang, G., Yin, R., 2019. A proxy for atmospheric daytime gaseous sulfuric acid concentration in

422   urban Beijing. Atmos. Chem. Phys. 19(3), 1971-1983.

423   Lyu, X. P., Guo, H., Cheng, H. R., Wang, D. W., 2018. New particle formation and growth at a suburban site and a background site in Hong

424   Kong. Chemosphere. 193, 664-674.

425   Ma, N., Zhao, C., Tao, J., Wu, Z., Kecorius, S., Wang, Z., Teich, M., 2016. Variation of CCN activity during new particle formation events

426   in the North China Plain. Atmos. Chem. Phys., 16(13), 8593-8607.

427   McGrath, M., Olenius, T., Ortega, I. K., Loukonen, V., Paasonen, P., Kurten, T., Kulmala, M., Vehkamaki H., 2012. Atmospheric Cluster

428   Dynamics Code: a flexible method for solution of the birth-death equations. Atmos. Chem. Phys. 12, 2345–2355.

429   McMurry, P. H., Fink, M., Sakurai, H., Stolzenburg, M. R., Mauldin III, R. L., Smith, J., Eisele, K.M., Sjostedt, S., Tanner, D., Huey, L.G.,

430   Nowak, J.B., Edgertoon, E., Voisin, D., 2005. A criterion for new particle formation in the sulfur‐rich Atlanta atmosphere. J.

431   Geophys. Res.: Atmos. 110(D22S02), 1-10

432   Meng, H., Zhu, Y., Evans, G. J., Jeong, C. H., Yao, X., 2015. Roles of SO2 oxidation in new particle formation events. J. Environ. Sci. 30,

433   90-101.

434   Metzger, A., Verheggen, B., Dommen, J., Weingartner, E., Riipinen, I., Kulmala, M., Spracklen, D.V., Carslaw, K.S., Baltensperger, Urs.,

435   2010. Evidence for the role of organics in aerosol particle formation under atmospheric conditions. Proc. Natl Acad. Sci. 107(15),

436   6646-6651.

437   Mikkonen, S., Romakkaniemi, S., Smith, J. N., Korhonen, H., Petaja, T., Plassduelmer, C., Boy, M., Mcmurry, P. H., Lehtinen, K. E. J.,

438   Joutsensaari, J., Hamed, A., Mauldin, R. L., Birmili, W., Spindler, G., Arnold, F., Kulmala, M., and Laaksonen, A., 2011, A statistical

439   proxy for sulphuric acid concentration. Atmos. Chem. Phys. 11(21), 11319-11334.

440   Napari, I., Noppel, M., Vehkamäki, H., Kulmala, M., 2002. An improved model for ternary nucleation of sulfuric acid–ammonia–water. J.

441   Chem. Phys. 116(10), 4221-4227.

442   Nieminen, T., Paasonen, P., Manninen, H. E., Sellegri, K., Kerminen, V. M., Kulmala, M., 2011. Parameterization of ion-induced nucleation

443   rates based on ambient observations. Atmos. Chem. Phys. 11(7), 3393-3402.

444   Ortega, I. K., Kurtén, T., Vehkam, Ki, H., Kulmala, M., 2008. The role of ammonia in sulfuric acid ion induced nucleation. Atmos. Chem.

445   Phys. 8(11), 2859–2867.

446   Paasonen, P., Nieminen, T., Asmi, E., Manninen, H. E., Petäjä, T., Metzger, A., 2010. On the roles of sulphuric acid and low-volatility

447   organic vapours in the initial steps of atmospheric new particle formation. Atmos. Chem. Phys. 10(22), 11223-11242..

448   Paasonen, P., Olenius, T., Kupiainen, O., Kurten, T., Petaja, T., Birmili, W., Hamed, A., Hu, M., Huey, L. G., Plassduelmer, C., Smith, J.

449   N., Wiedensohler, A., Loukonen, V., Mcgrath, M., Ortega, I. K., Laaksonen, A., Vehkamaki, H., Kerminen, V. M., Kulmala M.,

450   2012. On the formation of sulphuric acid – amine clusters in varying atmospheric conditions and its influence on atmospheric new

451   particle formation. Atmos. Chem. Phys. 12, 9113-9133.

452 Petäjä, T., Mauldin Iii, R. L., Kosciuch, E., McGrath, J., Nieminen, T., Paasonen, P., & Kulmala, M., 2009. Sulfuric acid and OH
453   concentrations in a boreal forest site. Atmos. Chem. Phys. 9(19), 7435-7448.

454 Peng, J. F., Hu, M., Wang, Z. B., Huang, X. F., Kumar, P., Wu, Z. J., Guo, S., Yue, D. L., Shang, D. J., Zheng, Z., He, L.Y., 2014. Submicron
455   aerosols at thirteen diversified sites in China: size distribution, new particle formation and corresponding contribution to cloud
456   condensation nuclei production. Atmos. Chem. Phys. 14(18), 10249-10265.

457 Pierce, J. R., I. Riipinen, M. Kulmala, M. Ehn, T. Petäjä, H. Junninen, D. R. Worsnop, and N. M. Donahue, 2011. Quantification of the
458   volatility of secondary organic compounds in ultrafine particles during nucleation events. Atmos. Chem. Phys. 11(17), 9019–9036,
459   doi:10.5194/acp-11-9019-2011.

460 Pöschl, U., 2005. Atmospheric aerosols: composition, transformation, climate and health effects. Angewandte Chemie International Edition.
461   44(46), 7520-7540.

462 Pöschl, U., 2011. Gas–particle interactions of tropospheric aerosols: Kinetic and thermodynamic perspectives of multiphase chemical
463   reactions, amorphous organic substances, and the activation of cloud condensation nuclei. Atmos. Res. 101(3), 562–573.

464 Qi, X., Ding, A., Roldin, P., Xu, Z., Zhou, P., Sarnela, N., Nie, W., Huang, X., Rusanen, A., Ehn, M., Rissanen, M.P., Petäjä, T., Kulmala,
465   M., Boy, M., 2018. Modelling studies of HOMs and their contributions to new particle formation and growth. Atmos. Chem. Phys.
466   18(16), 11779-11791.

467 Ran, L., Deng, Z.Z., Wang, P.C., Xia, X.A. 2016. Black carbon and wavelength-dependent aerosol absorption in the North China Plain
468   based on two-year aethalometer measurements. Atmos. Environ., 142, 132-144.

469 Roldin, P., Ehn, M., Theo Kurtén, Olenius, T., Rissanen, M., Sarnela, N., Elm, J., Rantala, P., Hao, L., Hyttinen, N., Heikkinen, L., Worsnop,
470   D. R., Pichelstorfer, L., Xavier, C., Clusius, P., Ostrom, E., Petaja, T., Kulmala, M., Vehkamaki, H., Virtanen, A., Riipinen, I., and
471   Boy, M., et al., 2019, The role of highly oxygenated organic molecules in the Boreal aerosol-cloud-climate system. Nature
472   Communications. 10(1), 1-15.

473 Setyan, A., Song, C., Merkel, M., Knighton, W. B., Onasch, T. B., Canagaratna, M.R., Worsnop, D.R., Wiedensohler, A., Shilling, J. E.,
474   Zhang, Q., 2014. Chemistry of new particle growth in mixed urban and biogenic emissions–insights from CARES. Atmos. Chem.
475   Phys. 14(13), 6477-6494.

476 Shilling, J. E., Zaveri, R. A., Fast, J. D., Alexander, M. L., Canagaratna, M.R., Fortner, E., Hubbe, J.M., Jayne, J.T., Sedlacek, A., Setyan,
477   A., Springston, S., Worsnop, D.R., Zhang, Q., 2013. Enhanced SOA formation from mixed anthropogenic and biogenic emissions
478   during the CARES campaign. Atmos. Chem. Phys. 13(4), 2091-2113.

479 Sihto, S. L., Kulmala, M., Kerminen, V. M., Maso, M. D., Petäjä, T., Riipinen, I., Korhonen, H., Arnold, F., Janson, R., Boy, M., Laaksonen,
480   A., Lehtinen, K.E.J., 2006. Atmospheric sulphuric acid and aerosol formation: implications from atmospheric measurements for
481   nucleation and early growth mechanisms. Atmos. Chem. Phys. 6(12), 4079-4091.

482 Sipilä, M., Berndt, T., Petäjä, T., Brus, D., Vanhanen, J., Stratmann, F., Patokoski, J., Mauldin, R.L., Hyvärinen, A.-P., Lihavainen, H.,
483   Kulmala, M., 2010. The role of sulfuric acid in atmospheric nucleation. Science. 327(5970), 1243-1246.

484 Sun, W., Shao, M., Granier, C., Liu, Y., Ye, C. S., & Zheng, J. Y., 2018. Long-Term Trends of Anthropogenic SO2, NOx, CO, and NMVOCs
485   Emissions in China. Earth's Future. 6(8), 1112-1133.

486 Vakkari, V., Tiitta, P., Jaars, K., Croteau, P., Beukes, J. P., Josipovic, M., Kerminen, V., Kulmala, M., Venter, A. D., Zyl, P. G. V., Laakso,
487   L., and Worsnop, D. R., 2015. Reevaluating the contribution of sulfuric acid and the origin of organic compounds in atmospheric
488   nanoparticle growth. Geophys. Res. Letters. 42(23), 10-486.

489   Wang, L., Xu, W., Khalizov, A. F., Zheng, J., Zhang, R., 2011. Laboratory investigation on the role of organics in atmospheric nanoparticle

490   growth. J. Phys. Chem. A. 115(32), 8940-8947.

491   Wang, Z. B., Hu, M., Sun, J. Y., Wu, Z. J., Yue, D. L., Shen, X. J., Zhang, Y. M., Pei, X. Y., Cheng, Y., Wiedensohler, A., 2013b.

492   Characteristics of regional new particle formation in urban and regional background environments in the North China Plain. Atmos.

493   Chem. Phys. 13, 12495–12506.

494   Wang, Z. B., Hu, M., Yue, D. L., He, L. Y., Huang, X. F., Yang, Q., Zheng, J., Zhang, R. Y., Zhang Y. H., 2013. New particle formation in

495   the presence of a strong biomass burning episode at a downwind rural site in PRD, China. Tellus B, 65, 1-10.

496   Wang, Z. B., Hu, M., Pei, X. Y., Zhang, R. Y., Paasonen, P., Zeng, J., Yue, D.L. Wu, Z.J., Boy, M., Wiedensohler, A., 2015. Connection of

497   organics to atmospheric new particle formation and growth at an urban site of Beijing. Atmos. Environ. 103, 7-17.

498   Wildt, J.; Mentel, T. F.; Kiendler-Scharr, A.; Hoffmann, T.; Andres, S.; Ehn, M.; Kleist, E.; Müsgen, P.; Rohrer, F.; Rudich, Y.; Springer,

499   M.; Tillmann, R.; Wahner, A., 2014. Suppression of new particle formation from monoterpene oxidation by NOx. Atmos. Chem.

500   Phys. 14, 2789−2804.

501   Wu, Z., Hu, M., Lin, P., Liu, S., Wehner, B., Wiedensohler, A., 2008. Particle number size distribution in the urban atmosphere of Beijing.

502   China. Atmos. Environ. 42(34), 7967-7980.

503   Wu, Z. J., Ma, N., Größ, J., Kecorius, S., Lu, K.D., Shang, D.J., Wang, Y,. Wu, Y.S., Zeng, L.M., Hu, M., Wiedensohler, A., Zhang, Y.H.,

504   2017. Thermodynamic properties of nanoparticles during new particle formation events in the atmosphere of North China Plain.

505   Atmos. Res. 188, 55-63.

506   Xiao, S., Wang, M. Y., Yao, L., Kulmala, M., Zhou, B., Yang, X., Chen, J.M., Wang, D.F., Fu, Q.Y., Worsnop, D.R., Wang, L., 2015. Strong

507   atmospheric new particle formation in winter in urban Shanghai, China. Atmos. Chem. Phys. 15(4), 1769-1781.

508   Yao, L., Garmash, O., Bianchi, F., Zheng, J., Kontkanen, J., Sipilä, M., 2018. Atmospheric new particle formation from sulfuric acid and

509   amines in a Chinese megacity. Science. 361, 6399, 278-281.

510   Yang, S., Liu, Z., Li, J., et al. 2021. Insights into the chemistry of aerosol growth in Beijing: Implication of fine particle episode formation

511   during wintertime. Chemosphere, 274,129776.

512   Yang, Y., Ji, D., Sun, J., Wang, Y., Yao, D., Zhao, S. M., Yu, X.N., Zeng, L.M., Zhang, H., Wang, Y. H., Wang, Y., 2019. Ambient volatile

513   organic compounds in a suburban site between Beijing and Tianjin: Concentration levels, source apportionment and health risk

514   assessment. Sci. Total Environ. 695, 133889.

515   Yu, H., Zhou, L., Dai, L., Shen, W., Dai, W., Zheng, J., Ma, Y., Chen, M., 2016. Nucleation and growth of sub-3 nm particles in the polluted

516   urban atmosphere of a megacity in China. Atmos. Chem. Phys. 16(4), 2641-2657.

517   Yu, H., Ren, L., Kanawade, V.P., 2017. New particle formation and growth mechanisms in highly polluted environments. Curr. Pollution

518   Rep. 3(4), 245-253.

519   Yue, D. L., Hu, M., Zhang, R. Y., Wang, Z. B., Zheng, J., Wu, Z.J.Wiedensohler, A. He, L.Y., Huang, X.F. Zhu, T., 2010. The roles of

520   sulfuric acid in new particle formation and growth in the megacity of Beijing. Atmos. Chem. Phys. 10(10), 4953-4960.

521   Zhang, H., Li, H., Zhang, Q., Zhang, Y., Zhang, W., Wang, X., and Yang, T., et al., 2017, Atmospheric volatile organic compounds in a

522   typical urban area of Beijing: Pollution characterization, health risk assessment and source apportionment. Atmos. 8(3), 61.

523   Zhang, Q., Stanier, C. O., Canagaratna, M. R., Jayne, J. T., Worsnop, D. R., Pandis, S. N., Jimenez, J., 2004. Insights into the chemistry of

524   new particle formation and growth events in Pittsburgh based on aerosol mass spectrometry. Environ. Sci. Technol. 38(18), 4797-

525   4809.

526   Zhang, Q., Zheng, Y., Tong, D., Shao, M., Wang, S., Zhang, Y., Xu, X., Wang, J., He, H., Liu, W., Ding, Y., Lei, Y., Li, J., Wang, Z., Zhang,
527   X., Wang, Y., Cheng, J., Liu, Y., Shi, Q., Yan, L., Geng, G., Hong, C., Li, M., Liu, F., Zheng, B., Cao, J., Ding, A., Gao, J., Fu, Q.,
528   Huo, J., Liu, B., Liu, Z., Yang, F., He, K., Hao, J., 2019. Drivers of improved PM$_{2.5}$ air quality in China from 2013 to 2017. Proc.
529   Natl Acad. Sci. 116 (49), 24463-24469.

530   Zhang, R. Suh, I., Zhao, J., Zhang, D., Fortner, E., Tie, X., Molina L. T., Molina, M. J., 2004. Atmospheric new particle formation enhanced
531   by organic acids. Science. 304, 1487-1490.

532   Zhang, R. Wang, L., Khalizov, A. F., Zhao, J., Zheng, J., Mcgraw, R., Molina, L. T., 2009. Formation of nanoparticles of blue haze enhanced
533   by anthropogenic pollution. Proc. Natl Acad. Sci., USA. 106, 17650-17654.

534   Zhang, R., Guo, S., Zamora, M. L., and Hu, M., 2015. Reply to Li et al.: Insufficient evidence for the contribution of regional transport to
535   severe haze formation in Beijing. Proc. Natl Acad. Sci. 112(21), E2741-E2741.
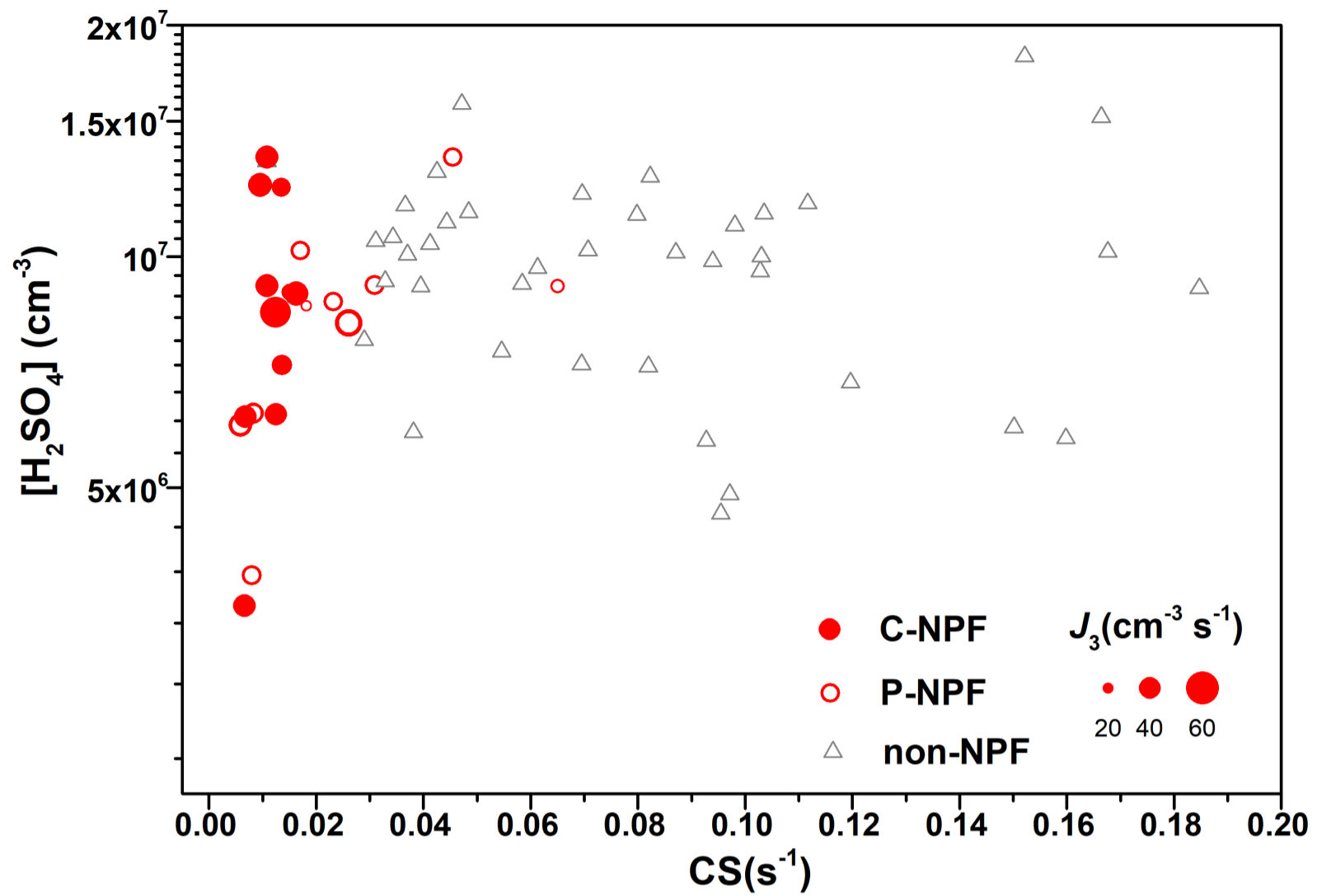
536

537
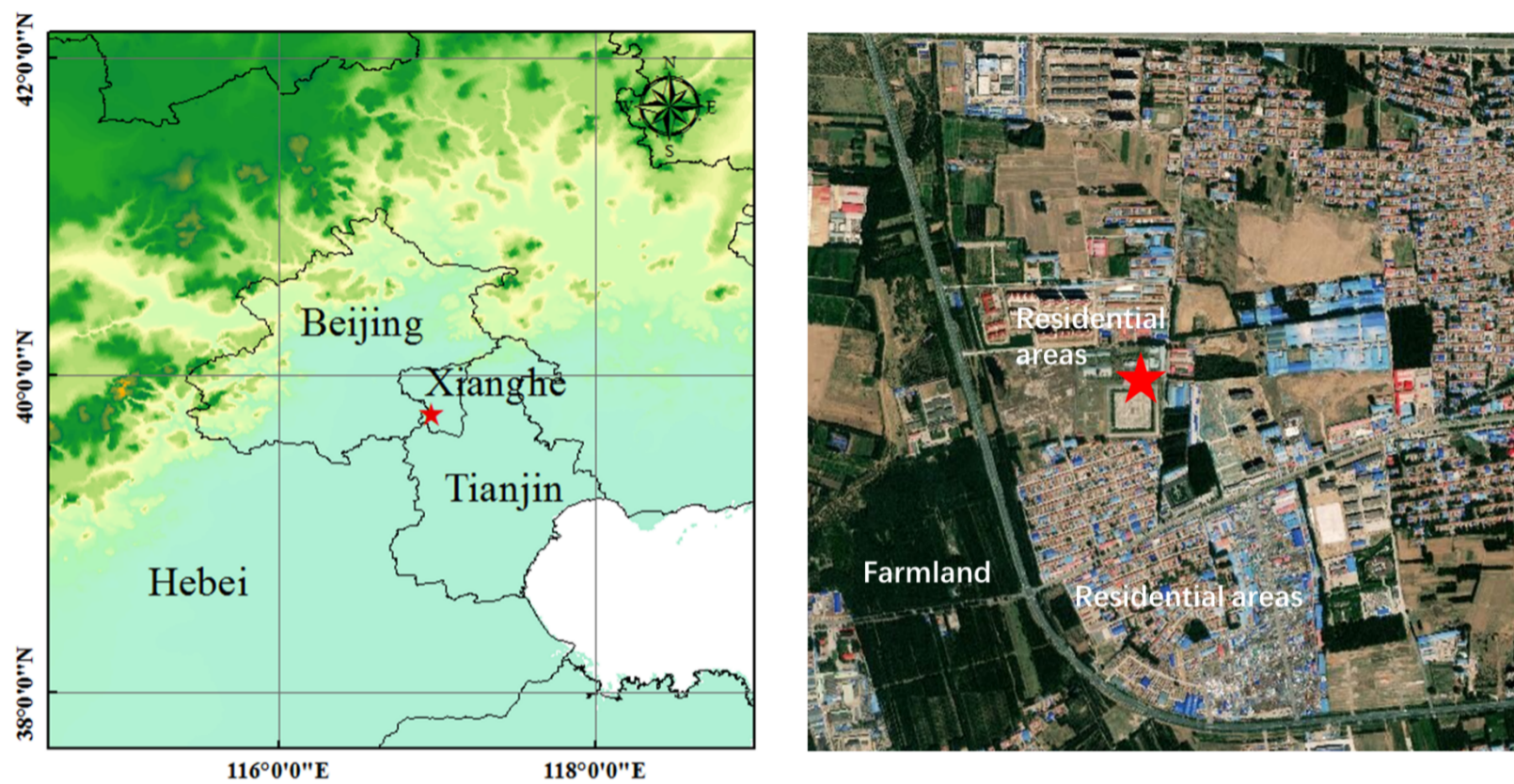
538
Figure 1. Location of the sampling site (Xianghe) in the North China Plain (Left) and the surrounding environments (Right)
540
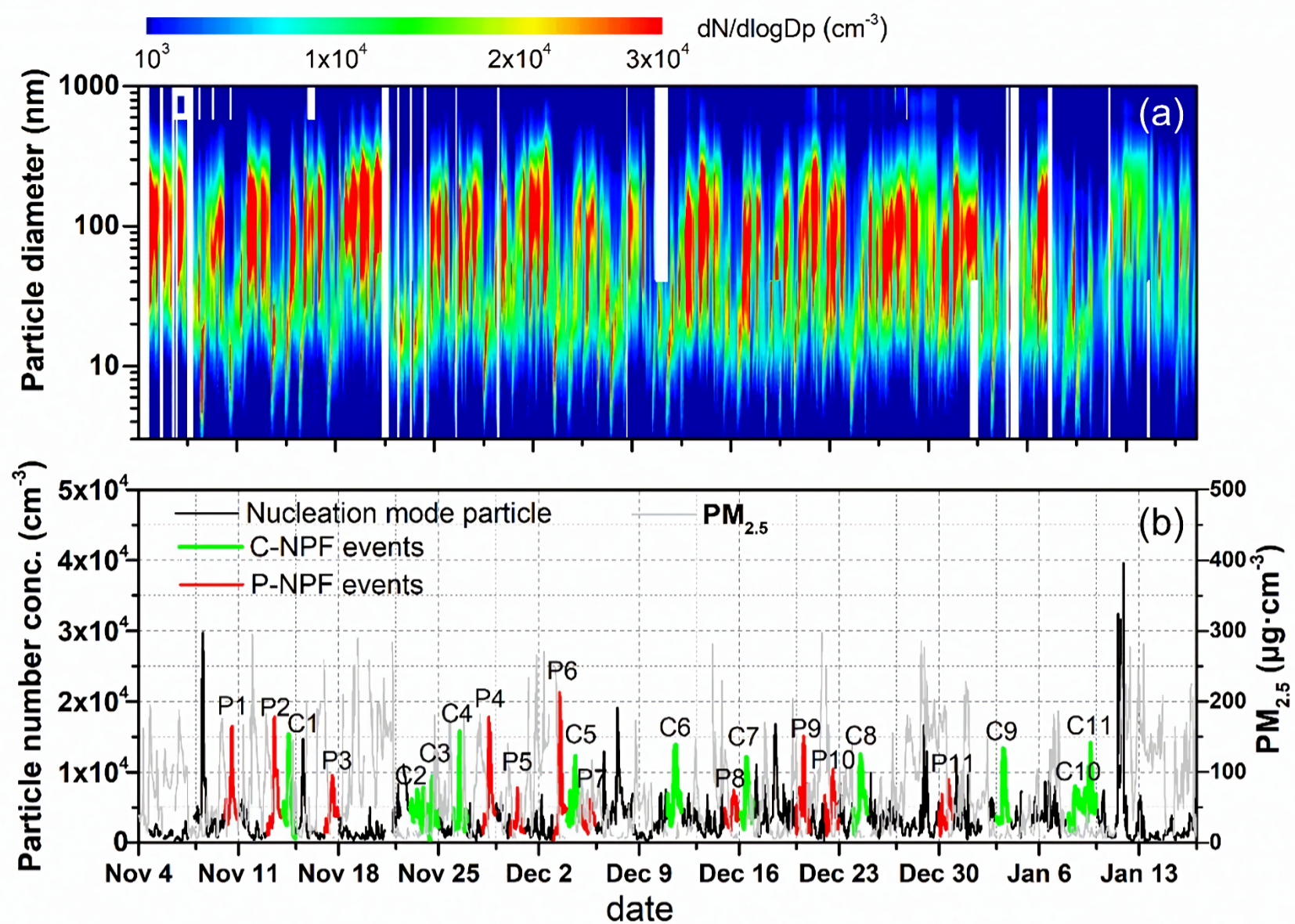
541

542 **Figure 2**. Variation in (a) particle number size distributions and (b) number concentration of nucleation mode particles during the winter

543 field campaign. The red-color line and green-color line denotes the occurrence of eleven P-NPF events (P1-P11) and eleven C-NPF events

544 (C1-C11).

545
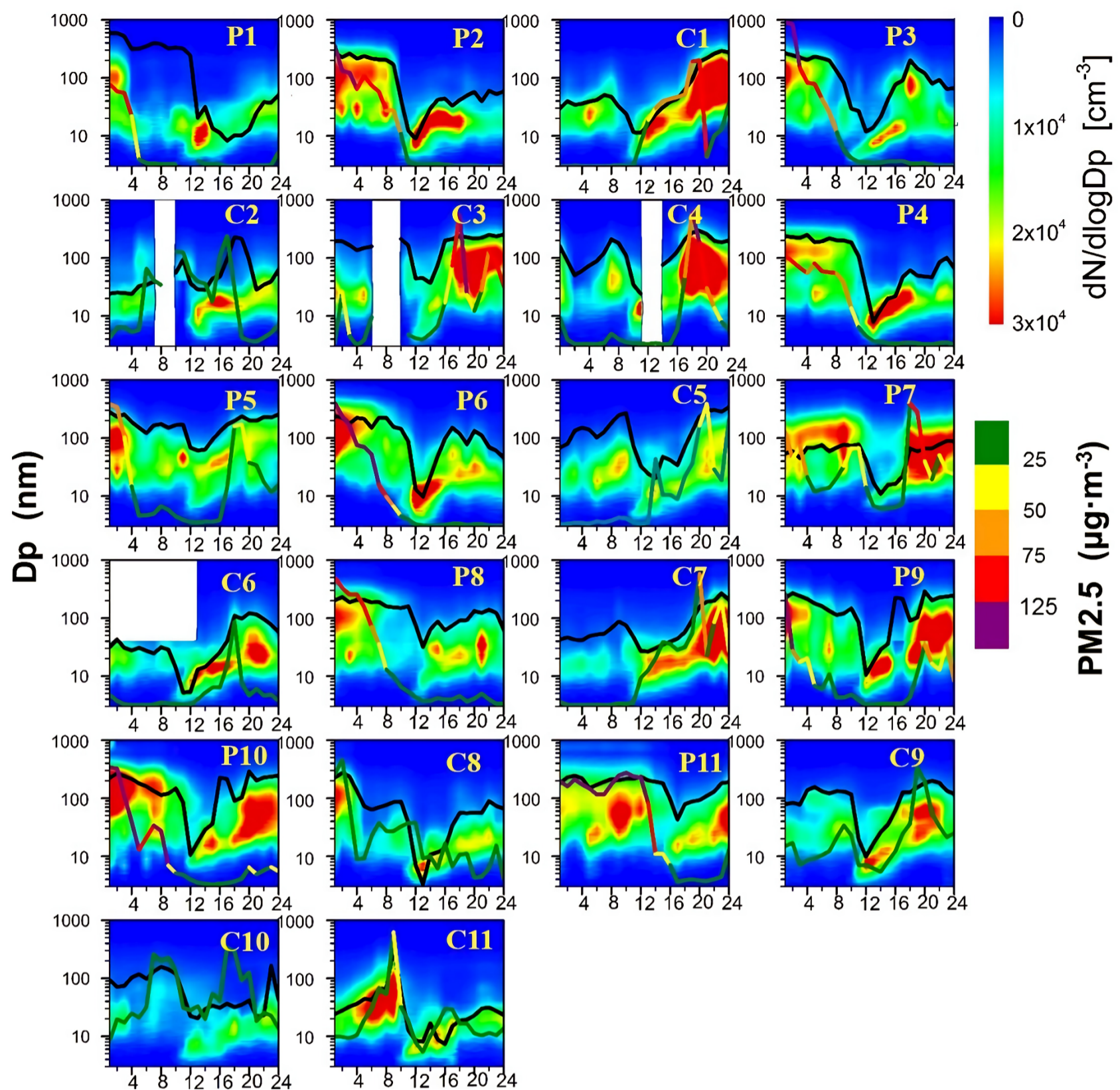
Figure 3. Particle number size distributions of the twenty-two NPF events. The P1-P11 and C1-C11 denote the eleven P-NPF and the eleven C-NPF events which are marked in Figure 2. The black dashed curve denotes the geometric mean diameter. The colors denote the PM$_{2.5}$ level (green: PM$_{2.5} \leq 25$ μg·m^{-3}, yellow: 26 μg·m^{-3} < PM$_{2.5} \leq 50$ μg·m^{-3}, orange: 51 μg·m^{-3} < PM$_{2.5} \leq 75$ μg·m^{-3}red, polluted periods, PM$_{2.5} > 150$ μg·m^{-3})

552

553

554 **Figure 4**. Relationship between CS and H_2SO_4 during the daytime for twenty-two NPF events and the non-NPF events. The solid circles,

555 hollow circles, and triangles represent C-NPF events, P-NPF events, and non-NPF events, respectively. The cycle size denotes the different

556 levels of formation rate (J_3).

557
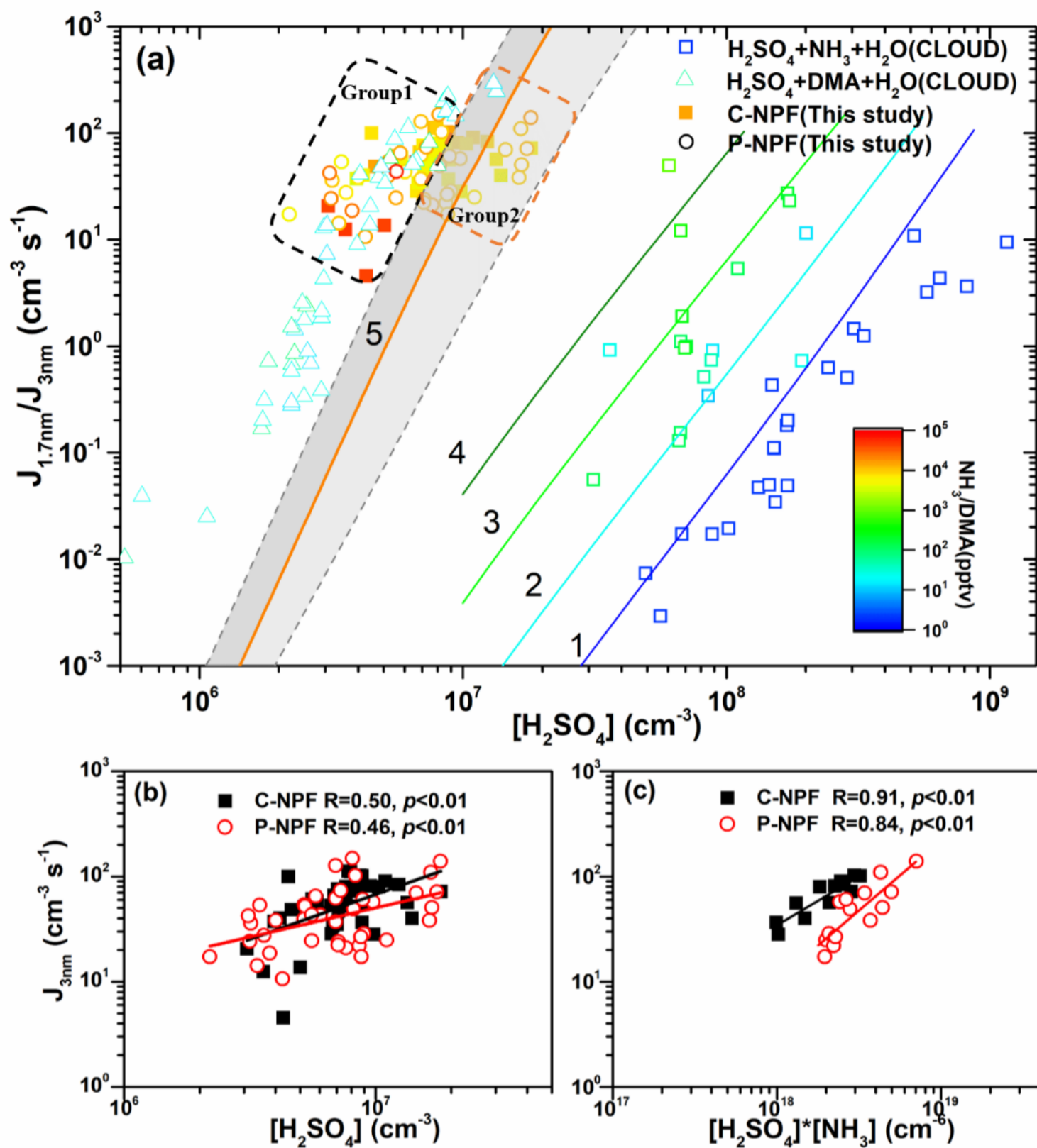
Figure 5. (a) Plot of atmospheric, experimental, and theoretical nucleation rates against H_2SO_4 concentration. The color code indicates the ammonia and DMA mixing ratio. Field observations in suburban Beijing are indicated by colored solid squares (C-NPF) and hollow cycles (P-NPF). The CLOUD data, recorded at 38% RH and 278 K, show $J_{1.7}$ with H_2SO_4, water, and different ammonia mixing ratio (2 pptv NH_3, curve 1; 10 pptv NH_3, curve 2; 100 pptv NH_3, curve 3; 1000 pptv NH_3, curve 4) in the chamber (colored open squares) (Kürten, 2019); The CLOUD data, recorded at 38% RH and 278 K, show $J_{1.7}$ with H_2SO_4, water, and different DMA mixing ratio (13-140 pptv DMA, colored triangles) (Almeida et al., 2013). Theoretical expectations (MALTE_BOX model) are indicated for H_2SO_4 nucleation with 10 pptv NH_3 (yellow line and grey band, curve 5), the bands correspond to the uncertainty range of the theory: +1 and -1 kcal·mol^{-1} binding energy. (b) Particle nucleation rate as a function of the H_2SO_4 concentration for the Group 1 and Group 2 events (c) Particle nucleation rates as a function of the H_2SO_4 and NH_3 concentration for the Group 2 events. R represents the Pearson's correlation coefficient and p represents the statistical significance level.
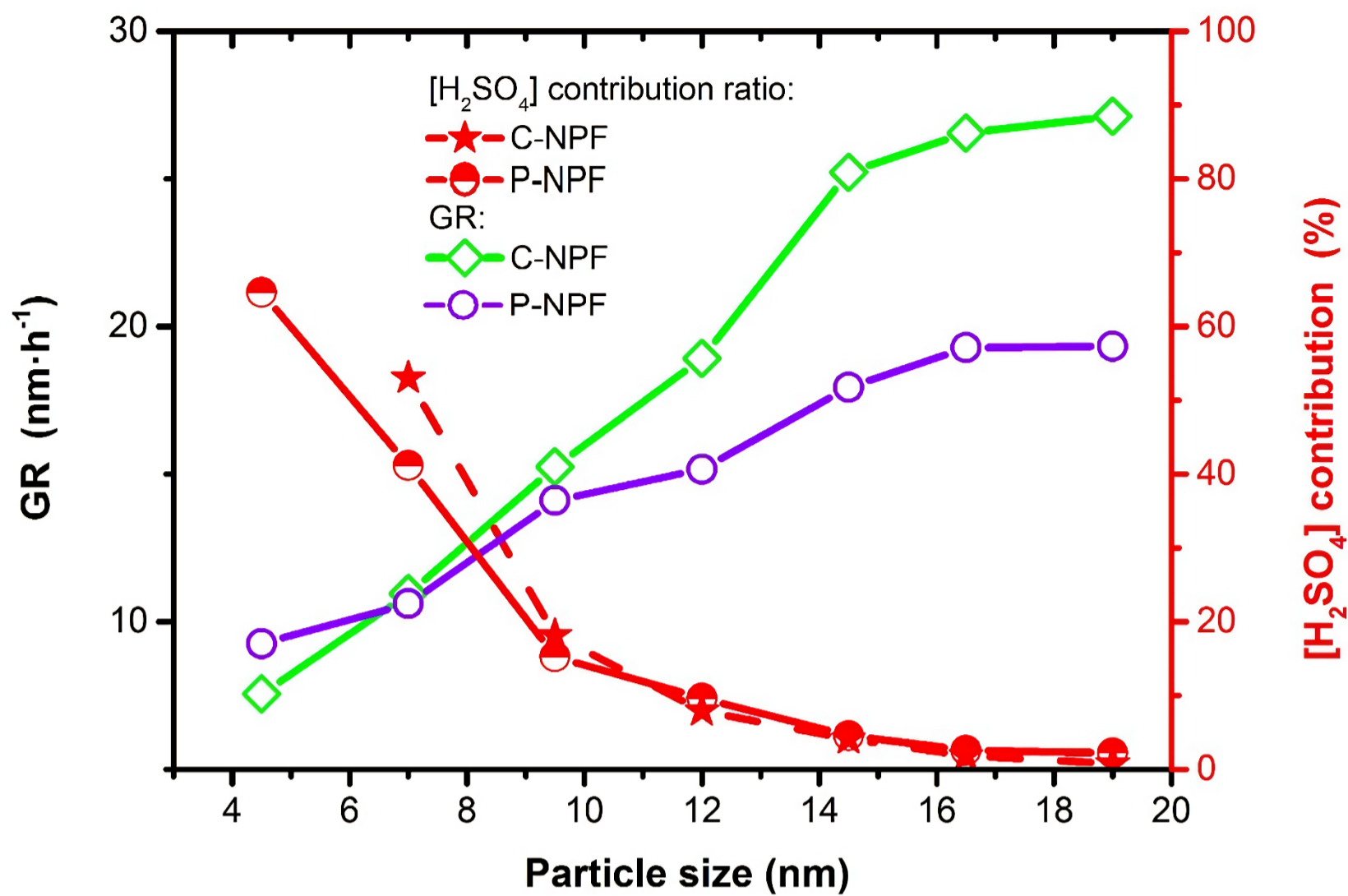
570

571   **Figure 6.** The size-dependent growth rate (GR) and the contributions of H_2SO_4 to the observed GR in the new particle growth stages.

572
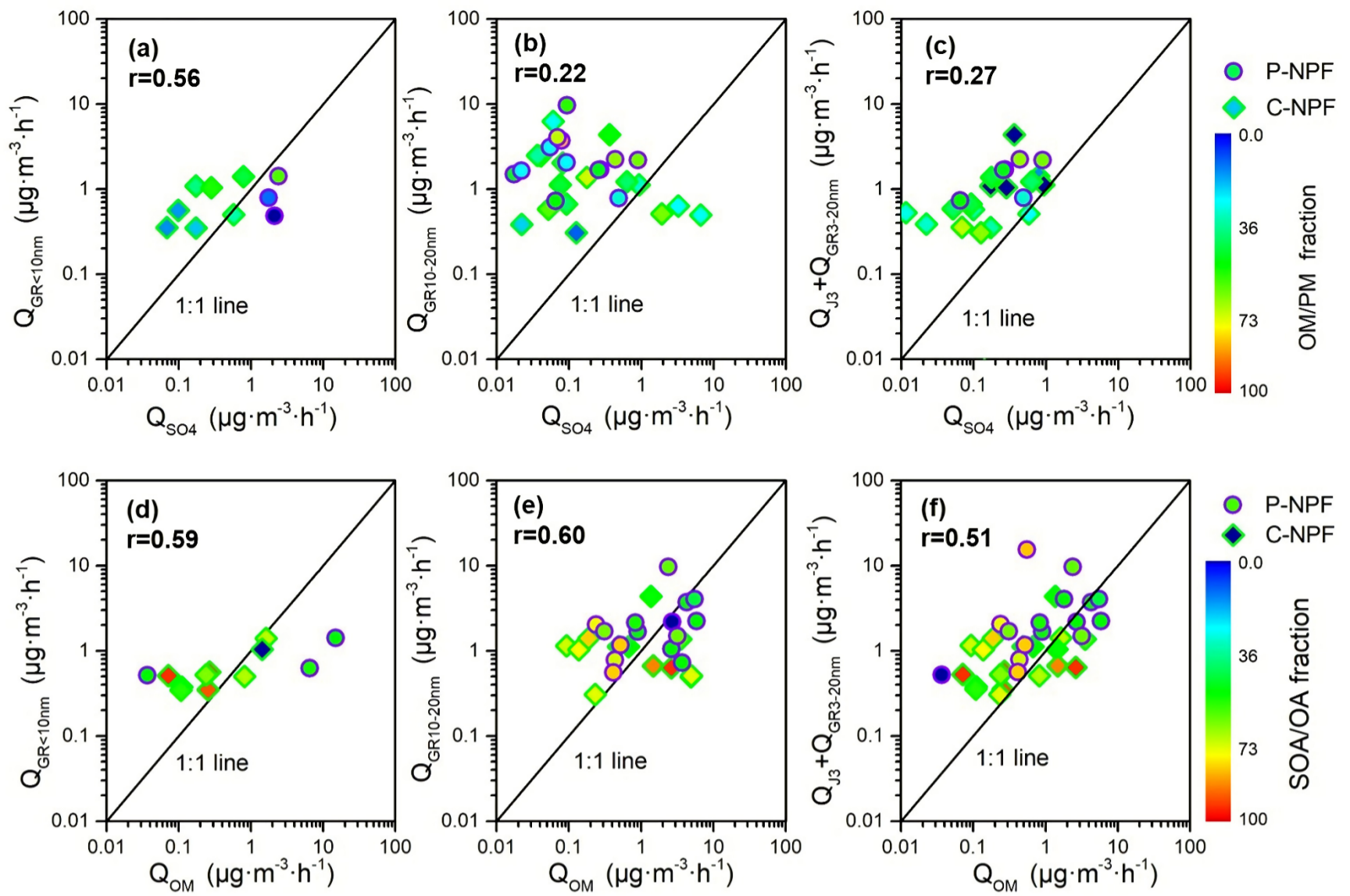
Figure 7. Observed Q_{SO4}, Q_{OM}, and Q_{GR} for different GR size ranges. (a, d) $Q_{GR<10nm}$ versus Q_{SO4} (or Q_{OM}) (b, e) $Q_{GR10-20nm}$ versus Q_{SO4} (or Q_{OM}) (c, f) The sum of $Q_{GR3-20nm}$ and Q_{J3} versus Q_{SO4} (or Q_{OM}).

577 **Table 1.** Summary of the average concentration of gaseous pollutants $PM_{2.5}$, meteorological parameters, and total particle number

578 concentration (PN) during the growth stage (09:00-16:00 h, local time) for NPF and non-NPF days.

Period	O_3	NO_X	NO_2	SO_2	$PM_{2.5}$	T	RH	WS	PN
	(ppbv)	(ppbv)	(ppbv)	(ppbv)	($\mu g \cdot m^{-3}$)	(°C)	(%)	($m \cdot s^{-1}$)	($\times 10^4$ cm^{-3})
C-NPF	24±8	9±3	7±2	1±2	12±5	2±3	18±4	4.5± 1.7	1.5± 0.4
P-NPF	22±7	16±15	11±5	2±2	24±20	6±4	20±7	3.7± 1.6	1.7± 0.6
NPF	23±7	13±12	9±5	2±2	18±16	4±4	19±6	4.1± 1.7	1.6± 0.5
non-NPF	22±10	42±37	24±14	7±5	58±47	5±5	31±18	1.9± 1.3	1.7± 1.3

579

580

581 **Table 2.** Summary of condensation sink (CS), concentration of NH_3 and sulfuric acid (H_2SO_4), particle formation rate (J_3), and particle
582 growth rate (GR) during the initial growth stage (09:00-12:00 h, local time) for NPF and non-NPF days.

Period	CS ($\times 10^{-2}$ s^{-1})	NH_3 (ppbv)	H_2SO_4 ($\times 10^6$ cm^{-3})	J_3 ($cm^{-3} \cdot s^{-1}$)	GR ($nm \cdot h^{-1}$)
C-NPF	1.2± 0.3	12.1±13.0	7.6± 3.0	58.6± 26.7	15.1± 6.8
P-NPF	2.5± 1.9	14.2± 12.4	7.9± 4.4	49.6±34.1	14.6± 5.1
non-NPF	8.1± 4.5		1.8 ± 1.9		

583

584